Jurnal Ilmu Fisika
Vol. 18, No. 2, September 2026, pp. 145–157
ISSN: 1979-4657 (Print); 2614-7386 (Online)
https://doi.org/10.25077/jif.18.2.145-157.2026

Jurnal Ilmu Fisika
Open Access

High-Concentration Synthesis of Ligand-Free Au and Ag Nanoparticles by Nanosecond Laser Ablation and Their Conversion to Au–Ag Alloy Nanoparticles via Femtosecond Laser Processing

Siti Masyithah[1,2], Muhandis Shiddiq[2*], Yessie Widya Sari[1]
[1] Physics Department, Faculty Mathematics and Natural Science, IPB University, Bogor, West Java 16680, Indonesia
[2] Research Center for Photonics, National Research and Innovation Agency (BRIN), Tangerang Selatan 15314, Indonesia

Article Info

Article History:

Received March 11, 2026
Revised July 3, 2026
Accepted July 16, 2026
Published online July 27, 2026

Keywords:

Laser ablation
Femtosecond processing
Au–Ag nanoparticles
Ligand-free synthesis
Colloidal stability

Corresponding Author:

Muhandis Shiddiq,
Email: muhandis.shiddiq@brin.go.id

ABSTRACT

A laser processing strategy is presented for the high-concentration synthesis of ligand-free Au, Ag, and Au–Ag alloy nanoparticles. Monometallic Au and Ag nanoparticles were first synthesized independently by nanosecond pulsed laser ablation in liquid (PLAL), producing stable ligand-free colloids. The Au and Ag colloids were then mixed in an equimolar ratio and irradiated with femtosecond laser pulses to induce alloy formation without chemical stabilizers or reducing agents. Ultraviolet–visible (UV–vis) spectroscopy shows a single localized surface plasmon resonance peak that shifts from 400 nm (Ag) to 509 nm (Au), with the Au–Ag alloy peak located between the two, confirming alloy formation. Transmission electron microscopy (TEM) reveals spherical Au, Au–Ag alloy, and Ag nanoparticles with average diameters of 11.8 ± 8.1 nm, 18.8 ± 5.9 nm, and 20.3 ± 9.4 nm, respectively, with the alloy nanoparticles exhibiting a narrower size distribution. Zeta potential measurements of −36.4, −41.2, and −48.1 mV for Ag, Au, and Au–Ag nanoparticles indicate good colloidal stability, with the alloy nanoparticles showing the highest stability. This laser-based approach provides a chemical-free route for producing high-concentration noble metal and alloy nanoparticles with tunable plasmonic and colloidal properties.

1. INTRODUCTION

Noble metal nanoparticles, particularly gold (AuNPs) and silver nanoparticles (AgNPs), have attracted significant attention because of their unique physicochemical and optical properties associated with localized surface plasmon resonance (LSPR). These nanoparticles exhibit strong light–matter interactions in the visible region, making them promising for a wide range of applications, including biosensing, catalysis, photothermal therapy, antimicrobial systems, and wound healing (Baygar et al., 2022; Damle et al., 2022; Fatmawati et al., 2023; Julita et al., 2022; Khan et al., 2022; Ruth et al., 2025; Sakthi Devi et al., 2022; Tang et al., 2020; Toczek et al., 2022; Tsalsabila et al., 2024; Zhu et al., 2023). AgNPs are known for their strong plasmonic response and pronounced antimicrobial activity, whereas AuNPs are widely used in biomedical and sensing applications due to their high chemical stability and biocompatibility (Anees Ahmad et al., 2020; Baygar et al., 2022; Damle et al., 2022; Franková et al., 2016; Mkhondwane & Pullabhotla, 2024; Padmos et al. 2015; Subha, 2021; Sudarman et al., 2023).

Despite these advantages, monometallic nanoparticles often show limited tunability in their optical and surface properties. For example, Ag nanoparticles provide strong plasmonic enhancement but may suffer from chemical instability, while Au nanoparticles offer superior stability but generally exhibit weaker plasmonic intensity than silver. These complementary characteristics have motivated the development of bimetallic nanoparticle systems that combine the desirable properties of both metals.

Among various bimetallic systems, Au–Ag nanoalloys have attracted considerable interest due to the synergistic interactions between Au and Ag atoms at the nanoscale. By integrating the strong plasmonic response of Ag with the chemical stability of Au, these nanoalloys exhibit tunable LSPR behavior, enhanced optical responses, and adjustable surface properties (Coviello et al., 2022; Nene et al., 2025). Consequently, Au–Ag nanoalloys have emerged as promising materials for applications in plasmonics, sensing, catalysis, and biomedicine (Lin et al., 2021; Masyithah et al., 2024; Mkhondwane & Pullabhotla, 2024; Padmos et al., 2015).

Chemical synthesis methods such as co-reduction and seed-mediated growth are commonly employed to produce Au–Ag nanoparticles (Nene et al., 2025; Situ et al., 2023). However, these approaches typically require reducing agents and stabilizing ligands, including citrate, polymers, or surfactants, to control nanoparticle growth and prevent aggregation. Although effective, the presence of surface-bound ligands may alter the intrinsic surface properties of nanoparticles, block active sites, and limit their performance in applications where direct surface interaction is important. In addition, residual chemical species may raise concerns related to environmental sustainability and biocompatibility (Zhang et al., 2020).

To overcome these limitations, pulsed laser ablation in liquid (PLAL) has emerged as a promising green synthesis technique for producing high-purity nanoparticles without chemical precursors or stabilizers (Kurniawan et al., 2022; Lazar et al., 2023; Zhang et al., 2017). In this method, high-energy laser pulses ablate a solid metal target immersed in liquid, generating ligand-free nanoparticles directly in the colloidal phase. PLAL has been successfully used to produce monometallic nanoparticles such as AgNPs and AuNPs with high purity.

Several recent studies have also reported the formation of Au–Ag alloy or bimetallic nanoparticles using nanosecond PLAL and related laser-based colloidal processing. Norsyuhada et al., (2018) synthesized Au–Ag alloy nanoparticles in deionized water using a Q-switched Nd:YAG PLAL technique, while Qayyum et al., (2022) reported a two-step laser-based approach in which surfactant-free Ag and Au nanoparticles were first produced by PLAL and subsequently irradiated as a mixed colloid using a nanosecond pulsed laser to form Au–Ag alloy nanoparticles. AdibAmini et al., (2023) further showed that the optical properties of Au/Ag bimetallic nanoparticles produced using 532 and 1064 nm pulsed laser ablation are strongly affected by laser wavelength and solution concentration. These studies demonstrate that nanosecond laser-based processing is a feasible route for Au–Ag alloy nanoparticle synthesis.

Despite these advances, the synthesis of bimetallic or alloy nanoparticles using PLAL remains challenging, particularly when high nanoparticle concentrations are required. Conventional approaches involving simultaneous or sequential ablation of different metal targets often produce mixtures of monometallic nanoparticles rather than well-defined alloy structures. Efficient atomic interdiffusion between nanoparticles is difficult to achieve under nanosecond laser conditions due to limited thermal interaction times.

In contrast, femtosecond laser irradiation introduces a distinct interaction regime characterized by ultrashort pulse duration and extremely high peak intensity, enabling non-equilibrium energy deposition and ultrafast thermal processes (Hidayah et al., 2022; Hidayah & Herbani, 2020). When applied to nanoparticle suspensions, femtosecond laser pulses can induce transient melting, reshaping, and enhanced atomic diffusion, which may promote alloy formation in mixed nanoparticle systems.

In this work, we propose a sequential nanosecond–femtosecond laser strategy for the formation of high-concentration Au–Ag nanoalloy nanoparticles. Monometallic AgNPs and AuNPs are first synthesized independently using nanosecond PLAL. The two colloids are then mixed in an equimolar ratio and subjected to femtosecond laser irradiation to induce alloy-like restructuring, resulting in the formation of Au-Ag nanoparticles. The optical properties, morphology, and colloidal stability of the

resulting nanoparticles are systematically investigated using UV–Vis spectroscopy, transmission electron microscopy (TEM), and zeta potential analysis.

2. METHODS

2.1 Materials

High-purity gold (Au) plate (99.99%, PT ANTAM Tbk, Indonesia) and silver (Ag) plate (99.95%, Silvergram brand supplied by PT Emas Perak Indonesia, Indonesia) were used as ablation targets for nanoparticle synthesis. Deionized (DI) water was employed as the liquid medium in all experiments. All glassware and quartz cuvettes were cleaned using a sequential oxidative acid-cleaning protocol prior to use to minimize contamination (Schmidt, 2022). No chemical precursors, reducing agents, or stabilizing ligands were introduced at any stage of the synthesis process, ensuring a fully ligand-free system.

2.2 Synthesis of Au and Ag Nanoparticles

Monometallic Au and Ag nanoparticles were synthesized separately using the pulsed laser ablation in liquid (PLAL) technique, following the general procedure reported by Nguyen et al., (2015) with minor modifications. A Nd:YAG laser operating at a fundamental wavelength of 1064 nm, with a pulse duration of 10 ns, repetition rate of 10 Hz, and pulse energy of 50 mJ, was used for ablation. The laser beam was focused onto the surface of the metal target immersed in 5 mL of deionized (DI) water. Laser ablation was performed until colloidal suspensions with high nanoparticle concentrations of approximately 4 μmol mL^{-1} were obtained. The concentration was estimated gravimetrically from the mass loss of each metal target after ablation relative to the liquid volume. The mass concentration was calculated as $C_{mg/mL} = \Delta m/V$, where Δm is the ablated mass in mg and V is the liquid volume in mL. The mass concentration was then converted to molar concentration using:

$$C_{\mu mol/mL} = \frac{C_{mg/mL} \times 1000}{M} \quad (1)$$

where M is the molar mass of Au or Ag in g mol^{-1}. Therefore, the reported concentration refers to the total metal-atom concentration in the colloidal suspension.

2.3 Alloying of Au–Ag Nanoparticles via Femtosecond Laser Irradiation

The alloying process was carried out following the methodology reported by Hidayah & Herbani, (2020), with several modifications. Colloidal AgNP and AuNP suspensions with high nanoparticle concentrations of approximately 4 μmol mL^{-1}, obtained from the PLAL process, were mixed in an equimolar ratio and transferred into a quartz cuvette. The mixed colloid was subsequently irradiated using a femtosecond Ti: sapphire laser system (Mai Tai, Spectra Physics) operating at a central wavelength of 800 nm, with a pulse duration of 100 fs (FWHM) and a repetition rate of 300 Hz.

The average output power of the femtosecond laser was set to 1.8 W. The laser beam was tightly focused using an aspheric lens with a focal length of 8 mm (numerical aperture, NA = 0.5) and directed perpendicular to the side wall of the quartz cuvette. The laser intensity at the focal point inside the solution was estimated to be on the order of 10^{14} W cm^{-2}. The colloidal mixture was irradiated until the Au and Ag nanoparticles were transformed into high-concentration Au–Ag alloy nanoparticles.

The alloy nanoparticles produced through this process are referred to as AuAg NPs, which originate from femtosecond laser irradiation of the equimolar AuNP–AgNP colloidal mixture. A schematic illustration of the experimental setup for both PLAL synthesis and femtosecond laser irradiation is shown in Figure 1.

2.4 Characterizations

The optical properties of the nanoparticle suspensions were characterized using UV–visible absorption spectroscopy (MayaPro 2000, Ocean Optics). The morphology and particle size of the nanoalloys were analyzed by transmission electron microscopy (TEM) using a FEI Tecnai 20G S-Twin microscope operated at an accelerating voltage of 200 kV. TEM samples were prepared by depositing

several drops of the nanoparticle suspension onto carbon-coated copper grids (Microgrid B, Okenshoji Co., Ltd.), followed by drying under vacuum at room temperature. Bright-field TEM images were analyzed using image analysis software to determine nanoparticle sizes. For each sample, at least 250 particles were measured from three different regions of the grid to obtain reliable size statistics. The zeta potential of the synthesized nanoalloys was measured in a 1 mM NaCl solution (pH = 6) using a Nano Partica SZ-100 zeta potential analyzer (Horiba, Ltd.), and the reported values represent the mean ± standard deviation of three independent measurements.

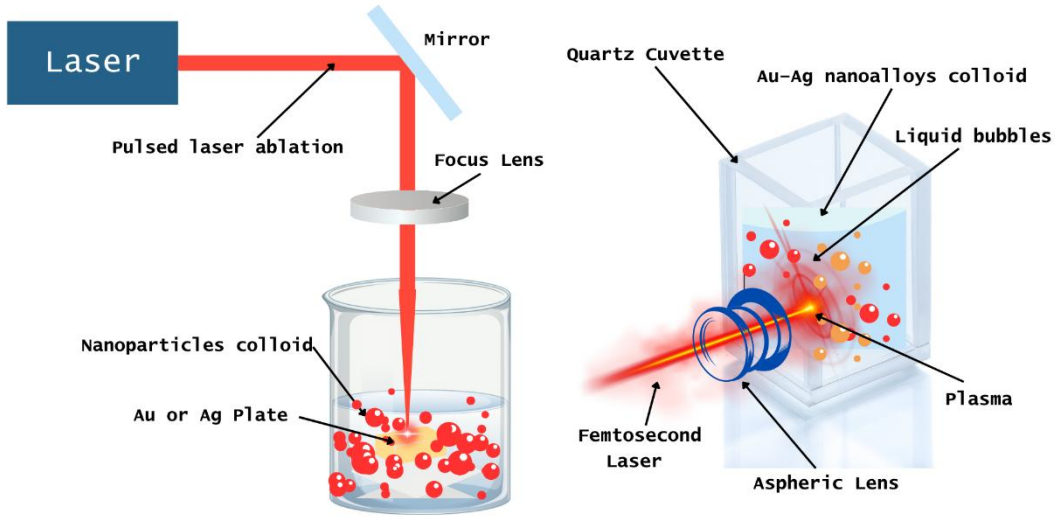

Figure 1. Schematic illustration of the experimental setup for the nanosecond-PLAL synthesis of monometallic Au and Ag nanoparticles, followed by femtosecond laser irradiation of the mixed colloidal suspension.

3. RESULTS AND DISCUSSION

3.1 Visual Appearance and Initial Observations

The visual appearance of colloidal nanoparticle suspensions provides an initial macroscopic indication of plasmonic behavior in noble metal nanoparticle systems. Figure 2 presents photographs of the ligand-free colloidal samples consisting of AgNPs, AuAg NPs, and AuNPs obtained from the laser synthesis.

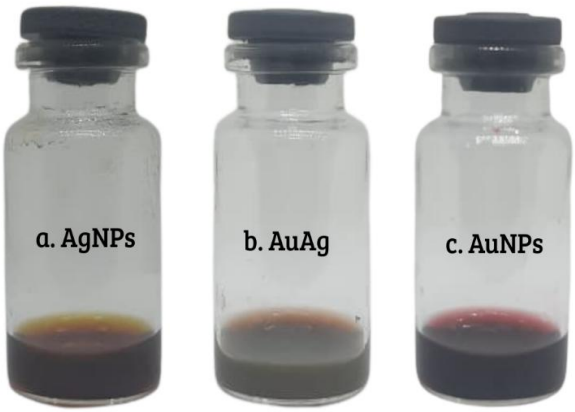

Figure 2. Photographs of ligand-free colloidal nanoparticles synthesized via sequential nanosecond–femtosecond laser processing. (a) AgNPs, (b) AuAg NPs obtained from an equimolar AgNP–AuNP mixture after femtosecond irradiation, and (c) AuNPs.

As shown in Figure 2a, the AgNP colloid exhibits a pale yellow–brown coloration, characteristic of the LSPR of silver nanoparticles (Pannerselvam et al., 2017). In contrast, the AuNP colloid (Figure 2c) displays a deep reddish color, which is typical for gold nanoparticles with LSPR centered in the visible red region (Chen et al., 2023). These two monometallic systems serve as visual references for assessing plasmonic changes in the alloyed samples.

After femtosecond laser irradiation of the mixed colloid prepared from an equimolar AgNP–AuNP mixture, the resulting sample, denoted as AuAg NPs (Figure 2b), exhibits a darker brown coloration that lies visually between those of AgNPs and AuNPs. This intermediate color indicates a modification of the plasmonic response compared with the monometallic nanoparticles.

The observed color change suggests that femtosecond laser irradiation induces optical restructuring in the mixed nanoparticle system. Importantly, the AuAg NPs colloid does not show obvious phase separation or rapid precipitation immediately after synthesis, indicating that the sequential laser process produces a macroscopically stable dispersion.

Although visual observation alone cannot confirm alloy formation at the nanoscale, the intermediate coloration of AuAg NPs relative to AgNPs and AuNPs provides qualitative evidence of plasmonic modification induced by femtosecond laser processing. These observations motivate further optical characterization using UV–Vis spectroscopy, discussed in the following section.

3.2 Optical Evolution and Alloy-Like Behavior of Au–Ag Nanoalloys

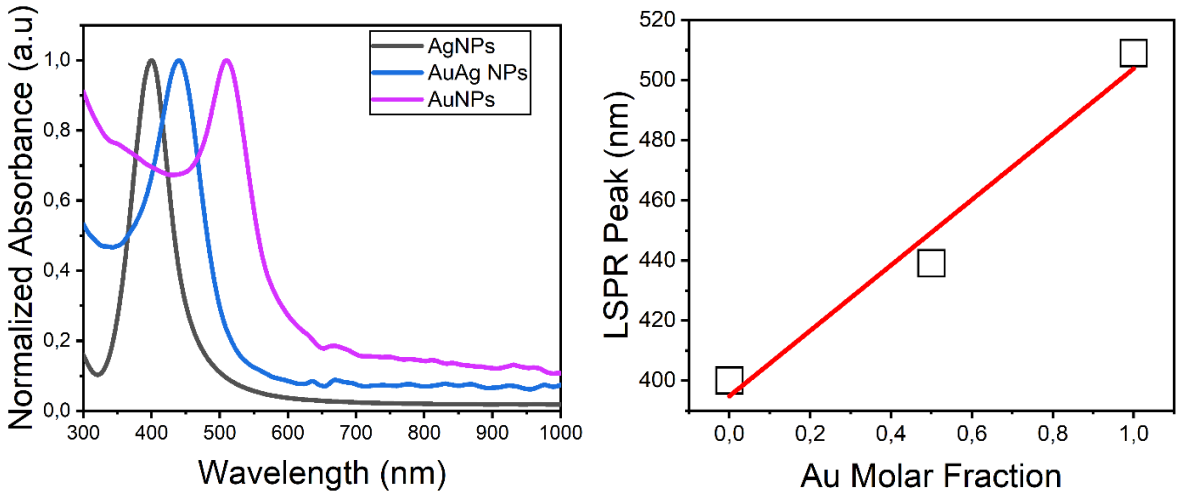

Figure 3. (a) Normalized UV–Vis absorption spectra of AgNPs ($x_{Au} = 0$), AuAg NPs ($x_{Au} = 0.50$), and AuNPs ($x_{Au} = 1.00$). (b) LSPR peak position as a function of Au molar fraction.

The optical properties of the synthesized nanoparticles were investigated using UV–Vis absorption spectroscopy to elucidate the plasmonic evolution induced by the sequential nanosecond–femtosecond laser process. Figure 3(a) presents the absorption spectra of AgNPs, AuAg NPs, and AuNPs, allowing direct comparison of their plasmonic responses. The corresponding LSPR peak positions and absorbance values as a function of Au molar fraction are summarized in Figure 3(b).

The AgNP colloid exhibits a dominant localized surface plasmon resonance (LSPR) peak centered at 400 nm, while the AuNP colloid shows a pronounced plasmon band at 509 nm. These peak positions are within the plasmonic range commonly observed for laser-synthesized Ag and Au nanoparticles and are used as reference points for evaluating alloy-like behavior in the mixed nanoparticle system (Dileseigres et al., 2022; Gezgin et al., 2017; Zhang et al., 2017).

After femtosecond laser irradiation of the equimolar AgNP–AuNP mixture, the resulting AuAg NPs exhibit a single dominant plasmon band centered at 439 nm, located between the characteristic LSPR peaks of AgNPs and AuNPs. The appearance of a single intermediate plasmon peak, rather than two distinct peaks corresponding to Ag and Au nanoparticles, indicates that the optical response cannot be attributed to a simple physical mixture of the two monometallic systems.

The relationship between plasmon resonance and composition is further illustrated in Figure 3(b), which shows the LSPR peak position as a function of Au molar fraction. AgNPs exhibit a plasmon peak near 400 nm, whereas AuNPs display a peak around 509 nm. The AuAg NPs sample, derived from the equimolar mixture, shows an intermediate peak at approximately 439 nm. This intermediate plasmon position follows the expected interpolation between Ag and Au resonances, which is characteristic of alloyed bimetallic nanoparticle systems and reflects the compositional dependence of the effective dielectric function of Au–Ag nanoalloys (Majhi & Kuiri, 2020; Papagiannouli et al., 2015).

To further distinguish alloy formation from a physical mixture, the UV–Vis spectrum of the AgNP–AuNP colloidal mixture prior to femtosecond irradiation was compared with that of the resulting AuAg NPs after irradiation (Figure 4). The initial mixed colloid displays two broadened spectral peaks arising from overlapping plasmon contributions of AgNPs and AuNPs. Following femtosecond laser irradiation, the spectrum evolves into a single dominant plasmon band corresponding to AuAg NPs. The collapse of the initially broadened dual-feature spectrum into a single dominant plasmon band also indicates the emergence of a unified plasmonic response, which is characteristic of alloy formation rather than the coexistence of separate monometallic nanoparticles. This spectral transformation indicates laser-induced alloy restructuring rather than simple coexistence of monometallic nanoparticles (Herbani et al., 2016; Hidayah et al., 2022).

Overall, the intermediate plasmon resonance observed for AuAg NPs relative to AgNPs and AuNPs provides strong optical evidence of alloy behavior induced by the sequential nanosecond–femtosecond laser strategy. These optical results are further elaborated by the morphological analysis obtained from TEM measurements, discussed in the following section.

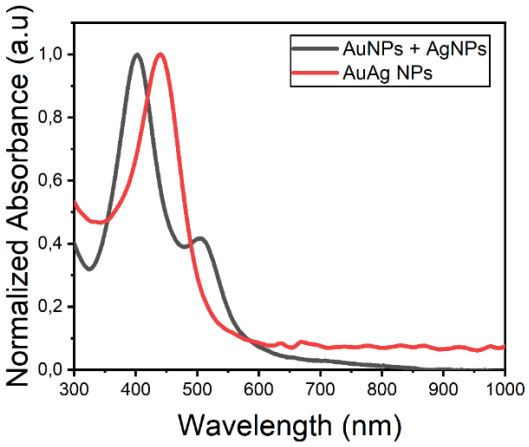

Figure 4. UV–Vis absorption spectra of the AgNP–AuNP physical mixture before irradiation and AuAg NPs after femtosecond laser irradiation.

3.3 Morphological Characteristics

Transmission electron microscopy (TEM) was performed to evaluate the morphology and size distribution of the monometallic nanoparticles and Au–Ag nanoalloys, providing direct structural evidence to complement the optical evolution discussed in Section 3.2. Representative TEM images of AgNPs and AuNPs synthesized by nanosecond PLAL are shown in Figure 5(a) and Figure 5(c), respectively, while the Au–Ag nanoalloys obtained after femtosecond laser irradiation are shown in Figure 5(b).

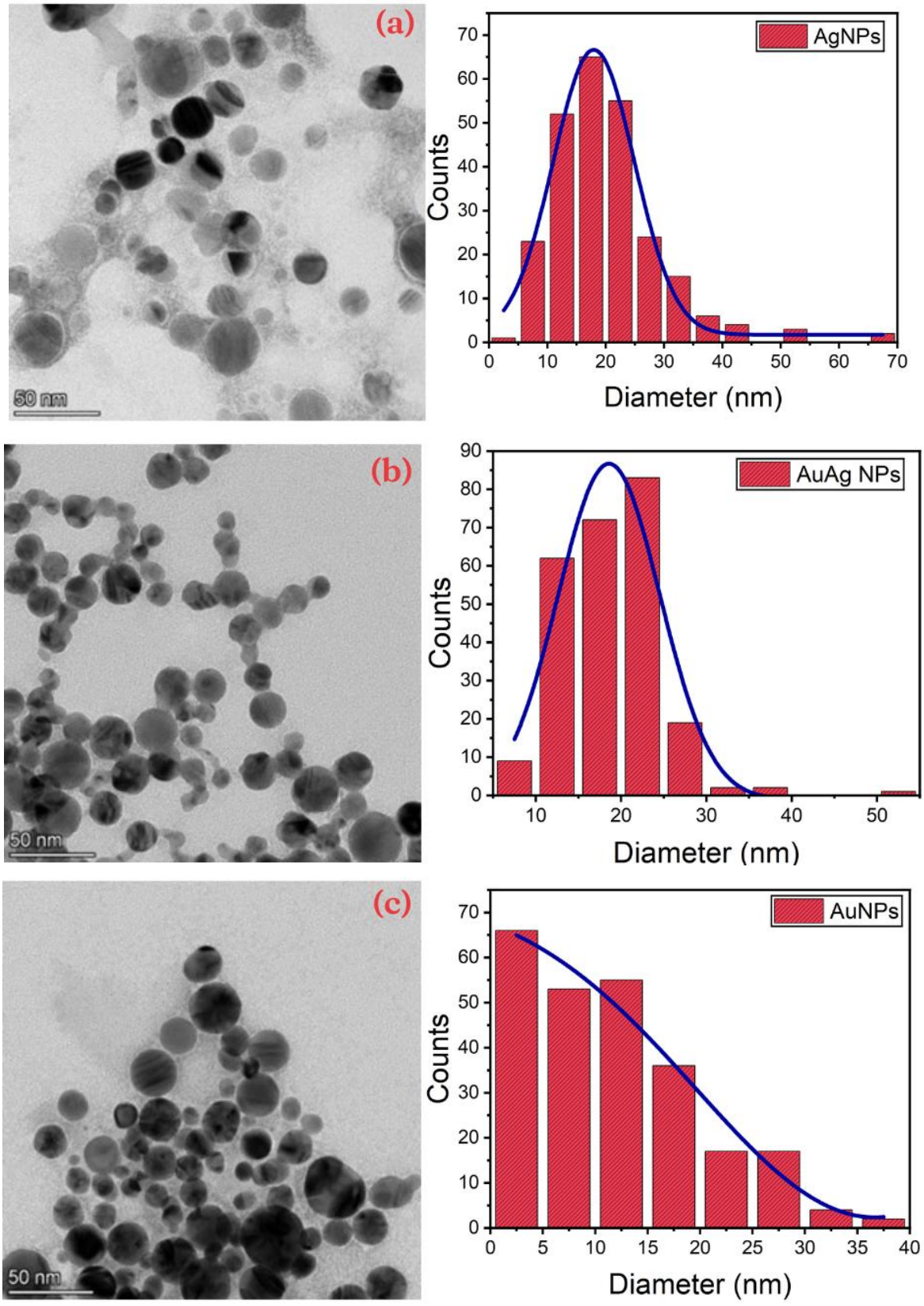

Figure 5. TEM images and particle size distributions of ligand-free nanoparticles: (a) AgNPs, (b) AuAg NPs, and (c) AuNPs. Insets show the corresponding particle size histograms obtained from TEM measurements.

The AgNPs exhibit predominantly quasi-spherical morphology with a broad size distribution and an average diameter of 20.26 ± 9.36 nm, whereas the AuNPs are smaller, with an average diameter of 11.81 ± 8.09 nm, but show relatively high polydispersity, as indicated by the large standard deviation compared with the mean diameter. This broad distribution is commonly associated with nanosecond PLAL, where nanoparticle formation involves rapid nucleation, growth, coalescence, fragmentation, and quenching in the ablation plume and cavitation bubble (Rehbock et al., 2014; Zhang et al., 2017). In comparison, the Au–Ag nanoalloy particles remain predominantly spherical and display an intermediate average diameter of 18.80 ± 5.86 nm. The corresponding particle size statistics are summarized in Table 1. The coefficient of variation decreased from 46.2% for AgNPs and 68.5% for AuNPs to 31.2% for AuAg NPs, indicating that femtosecond laser irradiation promoted partial size homogenization during alloy formation.

Table 1 Average particle diameter and standard deviation of monometallic and Au–Ag nanoalloy nanoparticles determined from TEM analysis.

Sample	Average diameter	Standard deviation
AgNPs	20.26	9.36
AuAg NPs	18.80	5.86
AuNPs	11.81	8.09

The LSPR peak positions can be further interpreted by considering the particle sizes obtained from TEM analysis. The AgNPs, with an average diameter of 20.26 ± 9.36 nm, exhibit an LSPR peak at 400 nm, whereas the smaller AuNPs, with an average diameter of 11.81 ± 8.09 nm, show a plasmon peak at 509 nm. The AuAg NPs have an intermediate average diameter of 18.80 ± 5.86 nm and display a single intermediate LSPR peak at 439 nm. Since the AuAg NPs are slightly smaller than the AgNPs but exhibit a red-shifted plasmon peak relative to AgNPs, the peak shift cannot be attributed to particle-size effects. Instead, the emergence of a single intermediate LSPR peak is mainly associated with alloy formation and the composition-dependent effective dielectric function of the Au–Ag system. Nevertheless, femtosecond-laser-induced reshaping and size homogenization may also contribute to minor size-related spectral changes. (Majhi & Kuiri, 2020; Papagiannouli et al., 2015; Rehbock et al., 2014).

The size of the Au–Ag nanoalloys indicates that femtosecond-laser-induced alloying in liquid is governed by a dynamical interplay of melting, interdiffusion, reshaping, coalescence, and fragmentation rather than by simple diameter averaging of the parent colloids. Because particle volume scales with the cube of the diameter, the larger Ag nanoparticles contribute more strongly to the final alloy-particle volume, which explains why the alloy size remains closer to that of Ag than to that of Au (Rehbock et al., 2014). Notably, the alloy nanoparticles also exhibit a narrower size distribution, suggesting that femtosecond post-irradiation promotes remelting-induced spherical reshaping and partial size homogenization (Rehbock et al., 2014).

Overall, the TEM results show that the sequential nanosecond–femtosecond laser strategy produces predominantly spherical nanoparticles while driving a clear structural evolution from monometallic colloids to more uniform Au–Ag nanoalloys.

3.4 Colloidal Stability

The colloidal stability of the ligand-free monometallic nanoparticles and Au–Ag nanoalloys was evaluated by zeta potential measurements, which provide insight into the electrostatic interactions governing dispersion stability in aqueous media. In ligand-free colloidal systems, zeta potential is particularly important because electrostatic repulsion is the primary mechanism preventing nanoparticle aggregation (Mateos et al., 2020; Rodriguez-Loya et al., 2023).

As summarized in Table 2, the AgNPs exhibit a zeta potential of −36.4 ± 0.1 mV, indicating good colloidal stability in water, while the AuNPs show a slightly more negative value of −41.2 ± 0.1 mV, reflecting stronger electrostatic stabilization. These values are consistent with previous reports on ligand-free noble-metal nanoparticles synthesized by pulsed laser ablation in liquid (Rehbock et al., 2014; Rodriguez-Loya et al., 2023).

The AuAg NPs exhibit the most negative zeta potential, −48.1 ± 0.1 mV, indicating the strongest electrostatic stabilization among the three samples. This more negative value may arise from the modified surface charge distribution after femtosecond-laser-induced alloying. In ligand-free nanoparticles produced by PLAL, negative zeta potential has been reported even without stabilizing ligands and may be related to plasma-induced surface charging rather than solely to surface oxides (Mateos et al., 2020; Dell'Aglio & De Giacomo, 2020). In Au–Ag bimetallic nanoparticles, alloying can also modify surface composition and interfacial physicochemical properties, as recent studies have shown Ag enrichment toward the surface of AuAg nanoparticles (Moreira et al., 2024). Therefore, the more negative zeta potential of AuAg NPs is attributed to the combined effects of laser-induced charging and alloy-related surface restructuring, which increases the effective negative surface charge density relative to the monometallic colloids.

Overall, the zeta potential analysis shows that the sequential nanosecond–femtosecond laser synthesis strategy yields a stable Au–Ag alloyed colloidal system with improved electrostatic stability compared with the corresponding monometallic nanoparticles.

Table 2 Zeta potential values of ligand-free monometallic and Au–Ag nanoalloy colloids measured in aqueous media.

Sample	Zeta Potensial (mV)
AgNPs	-36.4 ± 0.1
AuAg NPs	-48.1± 0.1
AuNPs	-41.2 ± 0.1

3.5 Proposed Mechanism for Sequential Nanosecond–Femtosecond Laser-Induced Alloying

Based on the combined optical, morphological, and colloidal-stability analyses, a mechanistic framework is proposed for the formation of ligand-free Au–Ag nanoalloys through the sequential nanosecond–femtosecond laser strategy, as schematically illustrated in Figure 6.

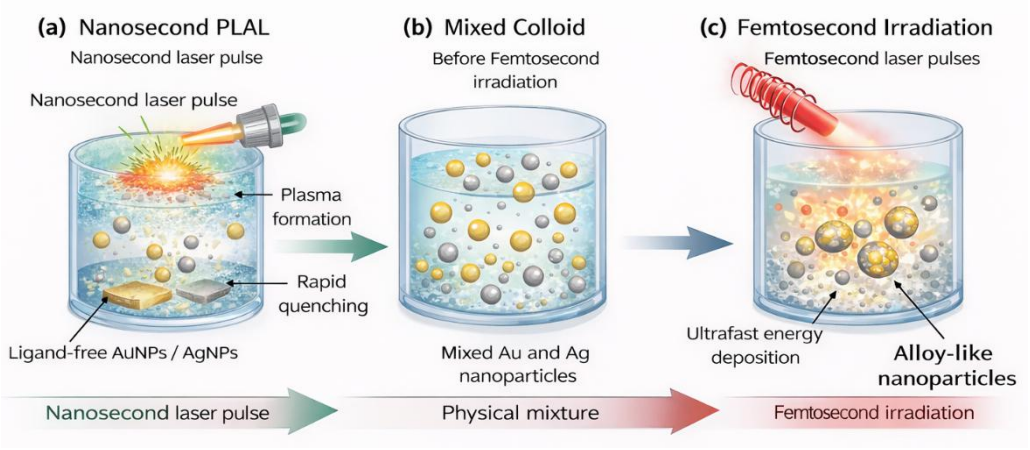

Figure 6. Proposed mechanism of Au–Ag alloy formation through nanosecond PLAL followed by femtosecond laser irradiation.

In the first stage, monometallic AgNPs and AuNPs are synthesized independently from their respective metal targets by nanosecond pulsed laser ablation in liquid (PLAL). During PLAL, high-energy laser pulses induce localized melting and vaporization of the target surface, followed by rapid quenching in the surrounding liquid, leading to the formation of high-purity, ligand-free colloidal nanoparticles (Amendola & Meneghetti, 2009; Zhang et al., 2017)

In the second stage, the two colloidal suspensions are mixed to form an equimolar AgNP–AuNP dispersion. At this point, the nanoparticles remain compositionally distinct, and the optical response of the mixed colloid is dominated by the combined plasmonic contributions of the individual Ag and Au nanoparticles.

The mixed colloid is then exposed to femtosecond laser irradiation, which introduces an ultrafast energy-deposition regime. Owing to the extremely short pulse duration and high peak intensity of the femtosecond pulses, rapid transient heating and localized melting are induced within the nanoparticles. These conditions enhance atomic mobility and facilitate interparticle diffusion, fusion, and compositional intermixing (Besner & Meunier, 2010; Hidayah et al., 2022).

As a consequence of these ultrafast processes, the initially separate Ag and Au nanoparticles undergo laser-induced alloying and structural reorganization, resulting in the formation of Au–Ag nanoalloys. This transformation is evidenced by the emergence of a single intermediate plasmon resonance in the UV–vis spectra and by the corresponding morphological features observed in the TEM analysis.

Overall, the sequential nanosecond–femtosecond laser approach combines the efficient nanoparticle generation capability of nanosecond PLAL with the ultrafast thermal and diffusional effects of femtosecond irradiation. This synergistic combination enables the formation of ligand-free Au–Ag nanoalloys from an equimolar mixture of monometallic colloids, offering a green and versatile route for the synthesis of plasmonically tunable noble-metal nanoparticle systems.

4. CONCLUSION

In this study, high-concentration ligand-free Ag, Au, and Au–Ag alloy nanoparticles were successfully synthesized using pulsed laser processing. Nanosecond pulsed laser ablation in liquid (PLAL) enabled the independent generation of high-purity monometallic AgNPs and AuNPs without the use of chemical stabilizers. Subsequent femtosecond laser irradiation of an equimolar AgNP–AuNP mixture induced alloying and structural reorganization, leading to the formation of Au–Ag alloy nanoparticles (AuAg NPs).

Optical characterization showed that the AuAg NPs exhibit a single localized surface plasmon resonance (LSPR) peak positioned between those of the AgNPs and AuNPs, indicating the intermediate plasmonic behavior characteristic of alloyed nanoparticle systems. Transmission electron microscopy further revealed that the AuAg NPs retain a predominantly spherical morphology, with particle sizes intermediate between those of the corresponding monometallic nanoparticles. In addition, zeta potential measurements demonstrated enhanced colloidal stability for the AuAg NPs relative to both AgNPs and AuNPs.

These findings demonstrate that sequential nanosecond–femtosecond laser processing provides an effective ligand-free route for producing high-concentration Au–Ag nanoalloys from an equimolar nanoparticle mixture. By combining the efficient nanoparticle generation capability of nanosecond PLAL with the ultrafast alloying effects of femtosecond laser irradiation, this approach offers a green and versatile strategy for tailoring the plasmonic and physicochemical properties of metal nanoparticle systems.

ACKNOWLEDGEMENT

This work was supported by research grants from the Ministry of Higher Education, Science, and Technology (Kemendiktisaintek), Republic of Indonesia. MS acknowledges support from the RP-ORNM funding program of the National Research and Innovation Agency (BRIN), Republic of Indonesia. SM acknowledges funding from the BRIN Degree by Research (BRIN DbR) program. The authors also acknowledge the facilities and technical support provided by the Advanced Characterization Laboratory, ELSA BRIN, Tangerang Selatan, Indonesia.

REFERENCE

AdibAmini, S., Sari, A. H., & Dorranian, D. (2023). Optical properties of synthesized Au/Ag Nanoparticles using 532 nm and 1064 nm pulsed laser ablation: Effect of solution concentration. *SN Applied Sciences*, *5*(4), 122. https://doi.org/10.1007/s42452-023-05310-1

Amendola, V., & Meneghetti, M. (2009). Laser ablation synthesis in solution and size manipulation of noble metal nanoparticles. *Physical Chemistry Chemical Physics*, *11*(20), 3805–3821. https://doi.org/10.1039/B900654K

Anees Ahmad, S., Sachi Das, S., Khatoon, A., Tahir Ansari, M., Afzal, Mohd., Saquib Hasnain, M., & Kumar Nayak, A. (2020). Bactericidal activity of silver nanoparticles: A mechanistic review. *Materials Science for Energy Technologies*, *3*, 756–769. https://doi.org/10.1016/j.mset.2020.09.002

Baygar, T., Saraç, N., & Uğur, A. (2022). Cytotoxicity and Wound Healing Capacity of Biologically Synthesized Silver Nanoparticles. *Mugla Journal of Science and Technology*, *8*(1), 63–68. https://doi.org/10.22531/muglajsci.1087581

Besner, S., & Meunier, M. (2010). Femtosecond Laser Synthesis of AuAg Nanoalloys: Photoinduced Oxidation and Ions Release. *The Journal of Physical Chemistry C*, *114*(23), 10403–10409. https://doi.org/10.1021/jp102461u

Chen, W., Chu, R., Li, H., Hua, T., Chen, H., Li, R., Zhou, D., Cao, S., Ye, S., & Li, H. (2023). A novel wound dressing based on a gold nanoparticle self-assembled hydrogel to promote wound healing. *Materials Advances*, *4*(14), 2918–2925. https://doi.org/10.1039/D3MA00130J

Coviello, V., Forrer, D., & Amendola, V. (2022). Recent Developments in Plasmonic Alloy Nanoparticles: Synthesis, Modelling, Properties and Applications. *ChemPhysChem*, *23*(21), e202200136. https://doi.org/10.1002/cphc.202200136

Damle, A., Sundaresan, R., Rajwade, J. M., Srivastava, P., & Naik, A. (2022). A concise review on implications of silver nanoparticles in bone tissue engineering. *Biomaterials Advances*, *141*, 213099. https://doi.org/10.1016/j.bioadv.2022.213099

Dell'Aglio, M., & De Giacomo, A. (2020). Plasma charging effect on the nanoparticles releasing from the cavitation bubble to the solution during nanosecond Pulsed Laser Ablation in Liquid. *Applied Surface Science*, *515*, 146031. https://doi.org/10.1016/j.apsusc.2020.146031

Fatmawati, T., Shiddiq, M., Armynah, B., & Tahir, D. (2023). Synthesis Methods of Fe_3O_4 Nanoparticles for Biomedical Applications. *Chemical Engineering & Technology*, *46*(11), 2356–2366. https://doi.org/10.1002/ceat.202200384

Franková, J., Pivodová, V., Vágnerová, H., Juráňová, J., & Ulrichová, J. (2016). Effects of Silver Nanoparticles on Primary Cell Cultures of Fibroblasts and Keratinocytes in a Wound-Healing Model. *Journal of Applied Biomaterials & Functional Materials*, *14*(2), 137–142. https://doi.org/10.5301/jabfm.5000268

Herbani, Y., Nakamura, T., & Sato, S. (2016). Spectroscopic monitoring on irradiation-induced formation of AuAg alloy nanoparticles by femtosecond laser. *AIP Conference Proceedings*, *1711*(1), 030005. https://doi.org/10.1063/1.4941620

Hidayah, A. N., & Herbani, Y. (2020). *Femtosecond laser melting and alloying in Au-Ag nanoalloys from colloid mixture of gold-silver nanoparticles*, *2256*(1), 020006. https://doi.org/10.1063/5.0018421

Hidayah, A. N., Herbani, Y., Steven, E., Subhan, A., Triyono, D., Isnaeni, Suliyanti, M. M., & Shiddiq, M. (2022). Tuning the electrical properties of colloidal nanoalloys by varying their composition. *Colloids and Surfaces A: Physicochemical and Engineering Aspects*, *641*, 128496. https://doi.org/10.1016/j.colsurfa.2022.128496

Julita, M., Shiddiq, M., & Khair, M. (2022). Determination of band gap energy of ZnO/Au nanoparticles resulting in laser ablation in liquid. *Indonesian Journal of Chemical Research*, *10*(2), 83–87.

Khan, Md. A. R., Al Mamun, M. S., Habib, Md. A., Islam, A. B. M. N., Mahiuddin, Md., Karim, K. Md. R., Naime, J., Saha, P., Dey, S. K., & Ara, M. H. (2022). A review on gold nanoparticles: Biological synthesis, characterizations, and analytical applications. *Results in Chemistry*, *4*, 100478. https://doi.org/10.1016/j.rechem.2022.100478

Kurniawan, Salamah, U., Herbani, Y., Isnaeni, & Shiddiq, M. (2022). Fabrication of Cu nanoparticles using pulsed laser ablation in ethylene glycol. *AIP Conference Proceedings*, *2652*(1), 020003. https://doi.org/10.1063/5.0107576

Lazar, O. A., Nikolov, A. S., Moise, C. C., Enachescu, M., Lazar, O. A., Nikolov, A. S., Moise, C. C., & Enachescu, M. (2023). Pulsed Laser Ablation in Liquids for Fabrication of Noble Metal Nanostructures. In *Laser Ablation—Applications and Modeling*. IntechOpen. https://doi.org/10.5772/intechopen.111550

Lin, Z., Luo, Y., Liu, P., Li, Y., Yue, J., & Jiang, L. (2021). Atomic-engineering Au-Ag nanoalloys for screening antimicrobial agents with low toxicity towards mammalian cells. *Colloids and Surfaces B: Biointerfaces*, *204*, 111831. https://doi.org/10.1016/j.colsurfb.2021.111831

Majhi, J. K., & Kuiri, P. K. (2020). Spectral Tuning of Plasmon Resonances of Bimetallic Noble Metal Alloy Nanoparticles Through Compositional Changes. *Plasmonics*, *15*(3), 797–804. https://doi.org/10.1007/s11468-019-01103-8

Masyithah, S., Alfaruqi, M. H., Yudasari, N., & Shiddiq, M. (2024). Fabrications of ZnO and Zn nanoparticles by pulsed laser ablation in water and acetone. *AIP Conference Proceedings*, *3003*(1), 020122. https://doi.org/10.1063/5.0186540

Mateos, H., Picca, R. A., Mallardi, A., Dell'Aglio, M., Giacomo, A. D., Cioffi, N., & Palazzo, G. (2020). Effect of the Surface Chemical Composition and of Added Metal Cation Concentration on the Stability of Metal Nanoparticles Synthesized by Pulsed Laser Ablation in Water. *Applied Sciences*, *10*(12). https://doi.org/10.3390/app10124169

Mkhondwane, S. T., & Pullabhotla, V. S. R. (2024). Synergistic effect in bimetallic gold catalysts: Recent trends and prospects. *Physical Sciences Reviews*, *9*(3), 1523–1551. https://doi.org/10.1515/psr-2022-0269

Moreira, M., Hillenkamp, M., Rodrigues, V., & Ugarte, D. (2024). Ag Surface Segregation in Sub-10-nm Bimetallic AuAg Nanoparticles Quantified by STEM-EDS and Machine Learning: Implications for Fine-Tuning Physicochemical Properties for Plasmonics and Catalysis Applications. *ACS Applied Nano Materials*, *7*(1), 1369–1378. https://doi.org/10.1021/acsanm.3c05495

Nene, A., Antarnusa, G., Dulta, K., Sadeghzade, S., Wang, L., Ravikumar, C. H., Aman, J., Khongthaw, B., Kandwal, A., Somani, P., Kumar, A., Ramachandran, K., Subramaniam, V., Galluzzi, M., Dou, S., & Liu, X. (2025). Au–Ag bimetallic nanoparticles: Synthesis, structure, and application in sensing. *ChemPhysMater*, *4*(4), 331–343. https://doi.org/10.1016/j.chphma.2025.02.006

Nguyen, T. B., Nguyen, T. D., Tran, T. D., & Thi, T. H. N. (2015). Laser-Induced Synthesis of Au–Ag Alloy Nanoparticles in Polyvinylpyrrolidone (C6H9NO)n Solution. *Journal of Cluster Science*, *26*(5), 1787–1799. https://doi.org/10.1007/s10876-015-0877-7

Norsyuhada, W., Shukri, W. M., Bidin, N., Islam, S., & Krishnan, G. (2018). Synthesis of Au-Ag Alloy Nanoparticles in Deionized Water by Pulsed Laser Ablation Technique. *Journal of Nanoscience and Nanotechnology*, *18*(7), 4841–4851. https://doi.org/10.1166/jnn.2018.15358

Padmos, J. D., Langman, M., MacDonald, K., Comeau, P., Yang, Z., Filiaggi, M., & Zhang, P. (2015). Correlating the Atomic Structure of Bimetallic Silver–Gold Nanoparticles to Their Antibacterial and Cytotoxic Activities. *The Journal of Physical Chemistry C*, *119*(13), 7472–7482. https://doi.org/10.1021/acs.jpcc.5b00145

Pannerselvam, B., Dharmalingam Jothinathan, M. K., Rajenderan, M., Perumal, P., Pudupalayam Thangavelu, K., Kim, H. J., Singh, V., & Rangarajulu, S. K. (2017). An *in vitro* study on the burn wound healing activity of cotton fabrics incorporated with phytosynthesized silver nanoparticles in male Wistar albino rats. *European Journal of Pharmaceutical Sciences*, *100*, 187–196. https://doi.org/10.1016/j.ejps.2017.01.015

Papagiannouli, I., Aloukos, P., Rioux, D., Meunier, M., & Couris, S. (2015). Effect of the Composition on the Nonlinear Optical Response of AuxAg1–x Nano-Alloys. *The Journal of Physical Chemistry C*, *119*(12), 6861–6872. https://doi.org/10.1021/jp512404a

Qayyum, H., Amin, S., Ahmed, W., Mohamed, T., Ur Rehman, Z., & Hussain, S. (2022). Laser-based two-step synthesis of Au-Ag alloy nanoparticles and their application for surface-enhanced Raman spectroscopy (SERS) based detection of rhodamine 6G and urea nitrate. *Journal of Molecular Liquids*, *365*, 120120. https://doi.org/10.1016/j.molliq.2022.120120

Rehbock, C., Jakobi, J., Gamrad, L., Meer, S. van der, Tiedemann, D., Taylor, U., Kues, W., Rath, D., & Barcikowski, S. (2014). Current state of laser synthesis of metal and alloy nanoparticles as ligand-free reference materials for nano-toxicological assays. *Beilstein Journal of Nanotechnology*, *5*(1), 1523–1541. https://doi.org/10.3762/bjnano.5.165

Rodriguez-Loya, J., Lerma, M., & Gardea-Torresdey, J. L. (2023). Dynamic Light Scattering and Its Application to Control Nanoparticle Aggregation in Colloidal Systems: A Review. *Micromachines*, *15*(1). https://doi.org/10.3390/mi15010024

Ruth, F., Soeratri, W., Hariyadi, D. M., Septiana, E., Muttaqien, S. E., Munfadlila, A. W., Sekaringtyas, F. C., & Rosyidah, A. (2025). Gold Nanoparticle Synthesized from Centella asiatica: Emphasis on Optimization, Characterization, Antioxidant, Antiglycation, and Cytotoxicity Effect as an Anti-aging Cosmetic Ingredient. *BioNanoScience*, *15*(1), 45. https://doi.org/10.1007/s12668-024-01713-5

Sakthi Devi, R., Girigoswami, A., Siddharth, M., & Girigoswami, K. (2022). Applications of Gold and Silver Nanoparticles in Theranostics. *Applied Biochemistry and Biotechnology*, *194*(9), Article 9. https://doi.org/10.1007/s12010-022-03963-z

Schmidt, H. G. (2022). Safe Piranhas: A Review of Methods and Protocols. *ACS Chemical Health & Safety*, *29*(1), 54–61. https://doi.org/10.1021/acs.chas.1c00094

Situ, X., Bayram, S. S., & Blum, A. S. (2023). Two-Step Synthesis of Large Gold–Silver Alloy Nanoparticles via the Combination of Seeded Growth and Citrate Co-reduction. *The Journal of Physical Chemistry C*, *127*(22), 10888–10895. https://doi.org/10.1021/acs.jpcc.3c03095

Subha, V. (2021). Silver Nanoparticles Impregnated Nanocollagen as Scaffold for Soft Tissue Repair-Synthesis, Characterization, and In vitro Investigation. *International Journal of Medical Nano Research*, *8*(1), 034. https://doi.org/10.23937/2378-3664.1410034

Sudarman, F., Shiddiq, M., Armynah, B., & Tahir, D. (2023a). Silver nanoparticles (AgNPs) synthesis methods as heavy-metal sensors: A review. *International Journal of Environmental Science and Technology*, *20*(8), 9351–9368. https://doi.org/10.1007/s13762-022-04745-0

Tang, J., Shi, H., Ma, G., Luo, L., & Tang, Z. (2020). Ultrasmall Au and Ag Nanoclusters for Biomedical Applications: A Review. *Frontiers in Bioengineering and Biotechnology*, *8*. https://www.frontiersin.org/articles/10.3389/fbioe.2020.01019

Toczek, J., Sadłocha, M., Major, K., & Stojko, R. (2022). Benefit of Silver and Gold Nanoparticles in Wound Healing Process after Endometrial Cancer Protocol. *Biomedicines*, *10*(3), 679. https://doi.org/10.3390/biomedicines10030679

Tsalsabila, A., Herbani, Y., & Widya Sari, Y. (2024). Investigation of pH effect on lysine-capped gold nanoparticles to induce hydroxyapatite formation. *AIP Conference Proceedings*, *3210*(1), 020004. https://doi.org/10.1063/5.0229963

Zhang, D., Gökce, B., & Barcikowski, S. (2017). Laser Synthesis and Processing of Colloids: Fundamentals and Applications. *Chemical Reviews*, *117*(5), 3990–4103. https://doi.org/10.1021/acs.chemrev.6b00468

Zhang, G., Ma, Y., Liu, F., Nie, Y., Liu, Z., Fu, X., Luan, X., Qu, F., Liu, M., & Zheng, Y. (2020). Seeded growth of gold–silver ultrathin wire–dot hybrid nanostructures. *CrystEngComm*, *22*(35), 5768–5775. https://doi.org/10.1039/D0CE01009J

Zhang, J., Chaker, M., & Ma, D. (2017). Pulsed laser ablation based synthesis of colloidal metal nanoparticles for catalytic applications. *Journal of Colloid and Interface Science, Laser Synthesis*, *489*, 138–149. https://doi.org/10.1016/j.jcis.2016.07.050

Zhu, B., Li, X., Li, Y., Liu, J., & Zhang, X. (2023). Boosting the Photocatalysis of Plasmonic Au-Cu Nanocatalyst by AuCu-TiO2 Interface Derived from O2 Plasma Treatment. *International Journal of Molecular Sciences*, *24*(13), 10487. https://doi.org/10.3390/ijms241310487